Cross-Linked and Uncross-Linked Biodegradable Nanocomposites. I. Nonisothermal Crystallization Kinetics and Gas Permeability

Y. F. Shih,[1] T. Y. Wang,[2] R. J. Jeng,[2] J. Y. Wu,[2] D. S. Wuu[3]

[1]*Department of Applied Chemistry, Chaoyang University of Technology, Wufong Township, Taichung County, 41319, Taiwan*
[2]*Department of Chemical Engineering, National Chung Hsing University, Taichung 402, Taiwan*
[3]*Department of Materials Engineering, National Chung Hsing University, Taichung 402, Taiwan*

Received 10 September 2007; accepted 11 May 2008
DOI 10.1002/app.28712
Published online 10 July 2008 in Wiley InterScience (www.interscience.wiley.com).

ABSTRACT: Various nanocomposites of poly(butylene succinates) (PBS) with different ratios of organically modified layered silicates (OMLS) were prepared. Moreover, such PBS nanocomposites cross-linked by dicumyl peroxide (DCP) were also prepared in this work. Effects of cross-linking and OMLS on nonisothermal crystallization kinetics and the gas permeability of PBS samples were investigated further. WAXD indicates that the layers of clay were intercalated by the modifiers, and that the interlayer distance of OMLS in the nanocomposites could be expanded to about 2.96 nm. The results of DSC analysis revealed that the crystallization temperatures of nanocomposites shifted to the lower temperature with the increase of OMLS content. With the addition of OMLS, crystallinity was decreased, whereas the half-life of crystallization was increased. On the other hand, even the cross-linked effects also increased the half-life of crystallization of the materials, but did not necessarily decrease crystallinity in all cases. Moreover, the PBS/OMLS nanocomposites showed a 23.87–46.64% decrease in permeability of oxygen when compared with the pristine PBS sample. Yet, the cross-linked nanocomposites exhibited decrements of 6.38–39.53%. This indicates that the gas permeability of PBS was more effectively depressed by the addition of OMLS than by the cross-linking reaction. The cross-linked structure of polymer seemed not to be very effective in decreasing the gas permeability of PBS. J Appl Polym Sci 110: 1068–1079, 2008

Key words: poly(butylene succinate); nonisothermal crystallization; organically modified layered silicates; nanocomposites; gas permeability

INTRODUCTION

The development of biodegradable polymeric materials with excellent properties has become the focus of highly active research worldwide because of the issue of environmental protection.[1] One of these biodegradable polymeric materials is poly(butylene succinate) (PBS) with the trade name of "Bionolle."[2] Recently, silicate layered polymer nanocomposites have been the focal point of both academic and industrial attention[3–5] because this type of nanocomposites often exhibits greatly enhanced physical and/or chemical properties with the addition of a smaller amount of silicate compared with conventional microscale composite materials. Polymer-layered silicate nanocomposites also show promising potential as barrier materials for a multitude of packaging applications.[6–8] Improvements in the gas barrier properties at low concentrations of the layered silicate (<5 wt %) have been reported.[9–14]

Moreover, the mechanical properties of vinyl polymer and PBS can be enhanced through the cross-linking reaction according to literatures.[15–17] In this work, various nanocomposites, consisting of PBS with different weight ratios of organoclay, were prepared by solution blending. Moreover, such PBS nanocomposites cross-linked by dicumyl peroxide (DCP) were also prepared in this work. Better mechanical and thermal properties of PBS were achieved by the addition of organoclay or the cross-linking reaction.[18,19] Recently, many researches have focused on the effects of organoclay or the cross-linking reaction on the crystallization behavior[20–22] and gas permeability[23,24] of biodegradable polymers due to the requisites for their final applications. The permeability (P) of polymers depends on both translational diffusion (D) and solubility (S) constants[25]:

$$P = D \times S \quad (1)$$

Correspondence to: Y. F. Shih (syf@cyut.edu.tw).
Contract grant sponsor: National Science Council; contract grant number: NSC 95-2221-E-324-055.
Contract grant sponsor: Education Ministry of Taiwan, ROC.

The translational diffusion (D) increases with temperature and the strength of the attractive interactions between the polymer and the permeant. Polymers which interact strongly with permeants favor permeability and conversely polymers interacting poorly with a given permeant will decrease permeation and therefore enhance the barrier properties of the composite. Moreover, permeability decreases with decreasing free volume of the polymer. Consequently, for a polymer, an increase in crystallinity, chain order, degree of cross-linking, or packing density, as well as compact morphology are all structural factors which would enhance the barrier properties.[14,15] Moreover, crystallization in a continuously varying environment is a practical necessity because industrial processes generally proceed under nonisothermal conditions.[20] The crystallization process affected by the dispersed layered silicates and cross-linking structure would be investigated under nonisothermal condition.

Nonisothermal crystallization kinetics

A number of models have been proposed to quantitatively analyze the crystallization kinetics during the nonisothermal process since the nonisothermal process is widely employed in current industry. These analyses are based on the theory of isothermal crystallization. For the isothermal crystallization, the process can be well described by Avrami equation[26]:

$$1 - X_t = \exp[-k(T)t^n] \quad \text{or} \quad 1 - X_t = \exp[-K(T)t]^n \tag{2}$$

where X_t is the relative crystallinity at the time t, $k(T)$ is the isothermal crystallization rate constant including nucleation and growth at temperature T, n is the Avrami constant, and $K(T)^n = k(T)$. The value of the Avrami constant n is directly related to the nucleation mechanism and crystal growth geometries. A great amount of works has been done on the nonisothermal crystallization. A number of models, such as Ozawa and modified Avrami methods have been proposed to analyze the kinetics crystallization quantitatively during the nonisothermal process.[26–31]

Ozawa method

To characterize the crystallization process, the differential scanning calorimetry (DSC) technique is usually utilized to measure the heat released from the sample because of the crystallization. The crystallinity, X_t, is obtained using DSC data based on the assumption that the evolution of crystallinity is linearly proportional to the evolution of heat released during the crystallization:

$$X_t = \int_{T_0}^{T} \left(\frac{dH_C}{dT}\right) dT \Big/ \int_{T_0}^{T_\infty} \left(\frac{dH_C}{dT}\right) dT \tag{3}$$

where H_c is the heat of crystallization, which is calculated from the integrated area of DSC peak of crystallization, and T_0 and T_∞ represent the onset and the end of crystallization temperatures, respectively.

One of the commonly used methods for analyzing nonisothermal crystallization kinetic process was proposed by Ozawa.[30] In a nonisothermal process, temperature changes with time, leading to the dependence of the crystallization rate on the time factor. The Ozawa Equation for a constant cooling rate (dT/dt, φ), is given by:

$$1 - X_t = \exp[-K(T)/\varphi^m] \tag{4}$$

$$\text{or} \quad \ln[-\ln(1 - X_t)] = \ln K(T) - m \ln \varphi \tag{5}$$

where $K(T)$ is the cooling function that depends on the growth geometry and the nucleation process, m is the Ozawa constant to describe the mechanism of nucleation and type of crystallization. The value of m and $K(T)$ can be obtained by fitting Ozawa plot, $\ln[-\ln(1 - X_t)]$ versus φ.[31]

Modified Avrami method

Based on isokinetic conditions and the assumption that the number of activated nuclei is a constant, Nakamura et al. extended the Avrami theory so that it could be applied to a nonisothermal crystallization process[32]:

$$1 - X_t = \exp\left[-\left(\int_0^t K(T)dt\right)\right]^n \tag{6}$$

where the integration variable is the time t whereas K appears to be a function of the temperature T only. So under nonisothermal conditions, eq. (6) is usually simplified as:

$$1 - X_t = \exp[-Z_t t^n] \tag{7}$$

$$\text{or} \quad \ln[-\ln(1 - X_t)] = \ln Z_t + n \ln t \tag{8}$$

This is the modified Avrami equation, where Z_t signifies the crystallization rate constant, n is the Avrami constant for describing the mechanism of nucleation and type of crystallization. The value of n and Z_t can be obtained by fitting the Avrami plot, $\ln[-\ln(1 - X_t)]$ versus $\ln t$. Furthermore, the final form of the parameter characterizing the kinetics of nonisothermal crystallization was provided by Jeziorny[33]:

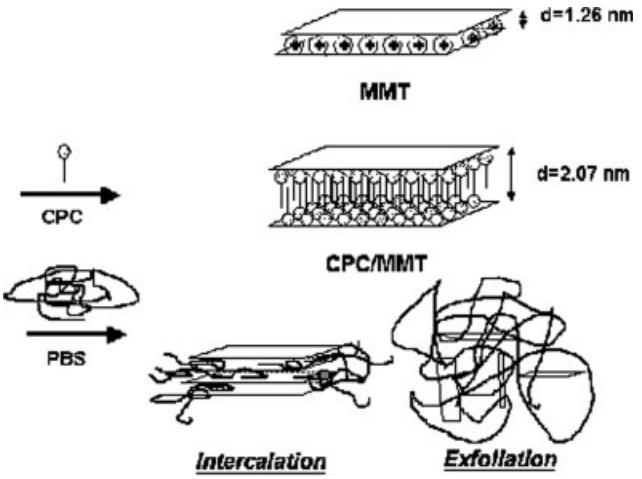

Scheme 1 The formation process of nanocomposites.

$$\ln Z_c = \ln Z_t/\varphi \quad (9)$$

In this work, we seek these detailed mechanisms by instrumental analysis and kinetic calculations. Moreover, the influence on the gas permeability will also be investigated.

EXPERIMENTAL

Materials

Montmorillonite "Kunipia F" clay was supplied by the Kunimine Co. of Tokyo, Japan. Bionolle#1001 [poly(butylene) succinate, PBS] is a commercial product of Showa Denko (Tokyo, Japan). OMLS were prepared by replacing Na^+ ions with cetyl pyridinium chloride (CPC) by means of ion exchange. Bionolle containing 1, 3, 5, 10 wt % of these OMLS (PBSMC1, PBSMC3, PBSMC5, PBSMC10, respectively) were prepared. Moreover, these nanocomposites were further cured by dicumyl peroxide (DCP) to obtain cross-linked nanocomposites (PBSDMC1, PBSDMC3, PBSDMC5, and PBSDMC10). In addition, PBS1D was the cross-linked PBS without OMLS. The formation process of these nanocomposites is shown in Scheme 1. The formulation of samples and possible cross-linking mechanism of PBS are shown in Table I and Scheme 2, respectively.

TABLE I
Formulation of Samples

	PBS	DCP	CPC/MMT
PBS	100	0	0
PBS1D	100	1	0
PBSMC1	100	0	1
PBSMC3	100	0	3
PBSMC5	100	0	5
PBSMC10	100	0	10
PBSDMC1	100	1	1
PBSDMC3	100	1	3
PBSDMC5	100	1	5
PBSDMC10	100	1	10

Characterization

X-ray diffractometry (XRD) measurements were carried out by using a Rigaku D/MAX-2200PC X-ray diffractometer (Cu Kα radiation, wavelength: $\lambda = 0.154$ nm) operated at 40 kV and 100 mA. Data were collected within the range of scattering angles (2θ) of $1.5 \sim 10^\circ$ X-ray diffractometry. Transmission electronic microscopy (TEM) images were obtained with a TEM 1200 CX-II instrument (JEOL, Tokyo, Japan) operated at an accelerating voltage of 120 kV to observe the nanoscale structures of various nanocomposites. Crystallization behavior was analyzed by differential scanning calorimeter (DSC; Seiko SII Model SSC5200). The nonisothermal crystallization was initiated by first heating the samples to 180°C for 5 min to eliminate previous thermal history. Subsequently, the samples were cooled at various constant rates of 5, 10, 20, 30, and 40°C min^{-1} to −30°C, respectively. The exothermic crystallization peak was then recorded as a function of temperature. Moreover, the morphology was observed with a

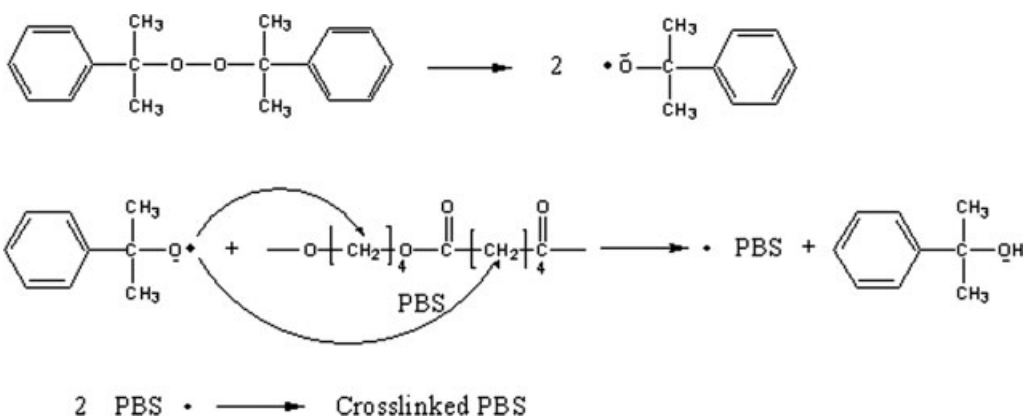

Scheme 2 The cross-linking mechanism of PBS.

TABLE II
WAXD Data for PBS Nanocomposites

	2θ	d-spacing (nm)
CPC/MMT	4.23	2.07
PBSMC1	3.12	2.83
PBSMC3	3.15	2.80
PBSMC5	3.11	2.84
PBSMC10	2.98	2.96
PBSDMC1	3.36	2.63
PBSDMC3	3.47	2.54
PBSDMC5	3.49	2.53
PBSDMC10	3.59	2.46

Carl Zeiss polarizing microscope, equipped with a Mettler Toledo hot-stage. The PBS samples were melted at 150°C for 5 min and then cooled down to 90°C at 5°C min^{-1}, for isothermal crystallization to occur. Oxygen permeation rates of the nanocomposites were measured using an OX-TRAN 2/61 (Mocon, Minneapolis, MN) at 25°C and 90% RH.

RESULTS AND DISCUSSION

Structure and morphology of the composites

The results of WAXD are shown in Figures 1–3 and Table II. The *d*-spacing of clay (MMT) and OMLS (CPC/MMT) are 1.26 and 2.07 nm (Fig. 1), respectively. Moreover, the patterns of uncross-linked PBS/OMLS composites (Fig. 2) indicate that the intensity of the *d*(001) peak shifted toward a lower diffraction angle with the addition of organoclay. A sharp peak obtained at $2\theta = 2.98^\circ$ (PBSMC10) indicates the formation of intercalated structure. This reveals that the interlayer spacing of organoclay in the nanocomposites was extended to about 2.96 nm (Table II). The increase in the *d*-spacing of the composites indicates that the PBS molecules were inserted into the interlayer spaces of the organoclay. Figure 3 shows the patterns of cross-linked PBS/OMLS composites. The intensity of the *d*(001) peak also shifted toward a lower diffraction angle with the addition of organoclay, but not as low as those of uncross-linked ones. This reveals that the interlayer spacings of organoclay in the nanocomposites were extended to about 2.46–2.63 nm (Table II). The interlayer spacings of organoclay in the cross-linked nanocomposites are smaller than those in the uncross-linked ones. This indicates that it is more difficult for the cross-linked PBS molecules to be inserted into the interlayer spaces of the organoclay, compared with that of the pristine PBS sample.

Moreover, coexistence of the intercalation and exfoliation structures in the uncross-linked and cross-linked nanocomposites (PBSMC5 and PBSDMC5) was further confirmed through TEM images, as shown in Figures 4 and 5. Nanometer-ranged intercalation and exfoliation clay tactoids were observed in both figures.

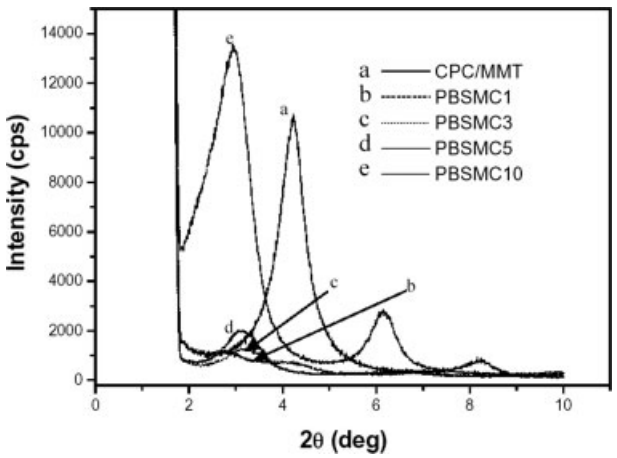

Figure 2 WAXD patterns of PBSMC nanocomposites.

Analysis of crystallization behavior

From the DSC thermograms, the initial temperature of crystallization was decreased with the increasing

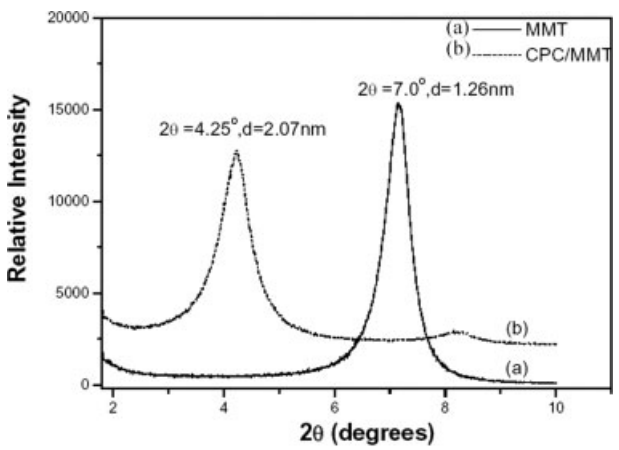

Figure 1 WAXD patterns of MMT and CPC/MMT.

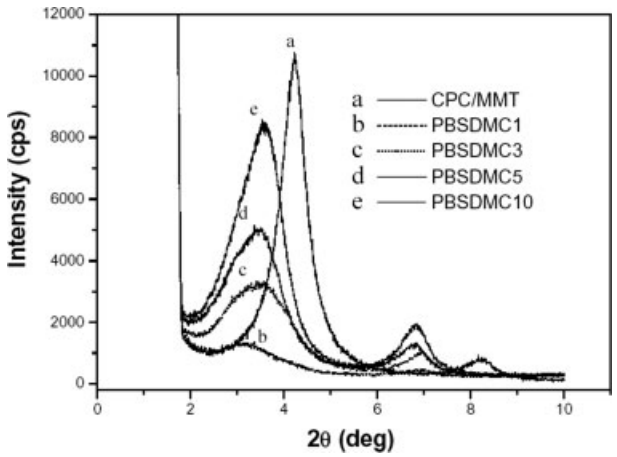

Figure 3 WAXD patterns of PBSDMC nanocomposites.

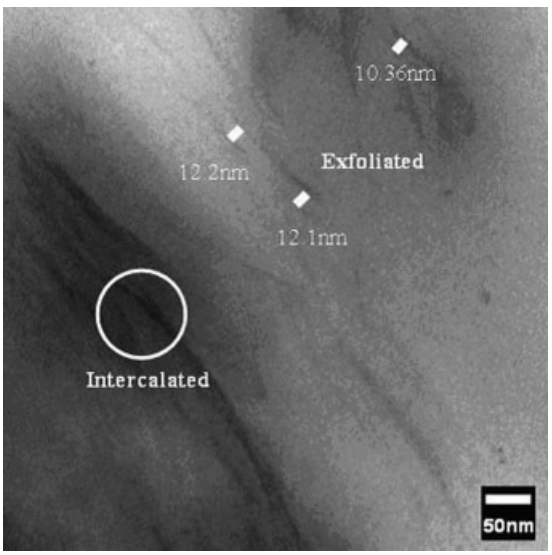

Figure 4 TEM photograph of PBSMC5.

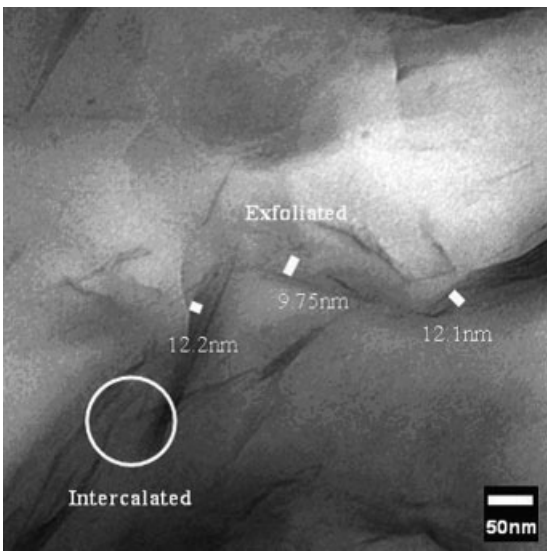

Figure 5 TEM photograph of PBSDMC5.

cooling rate for the pristine PBS sample [Fig. 6(a)]. This phenomenon was also observed in the crystallization process of the other samples [Fig. 6(b–d)]. Moreover, for the cross-linked samples [Fig. 6(b,d)], the initial temperatures of crystallization were lower than those of uncross-linked ones [Fig. 6(a,c)] while

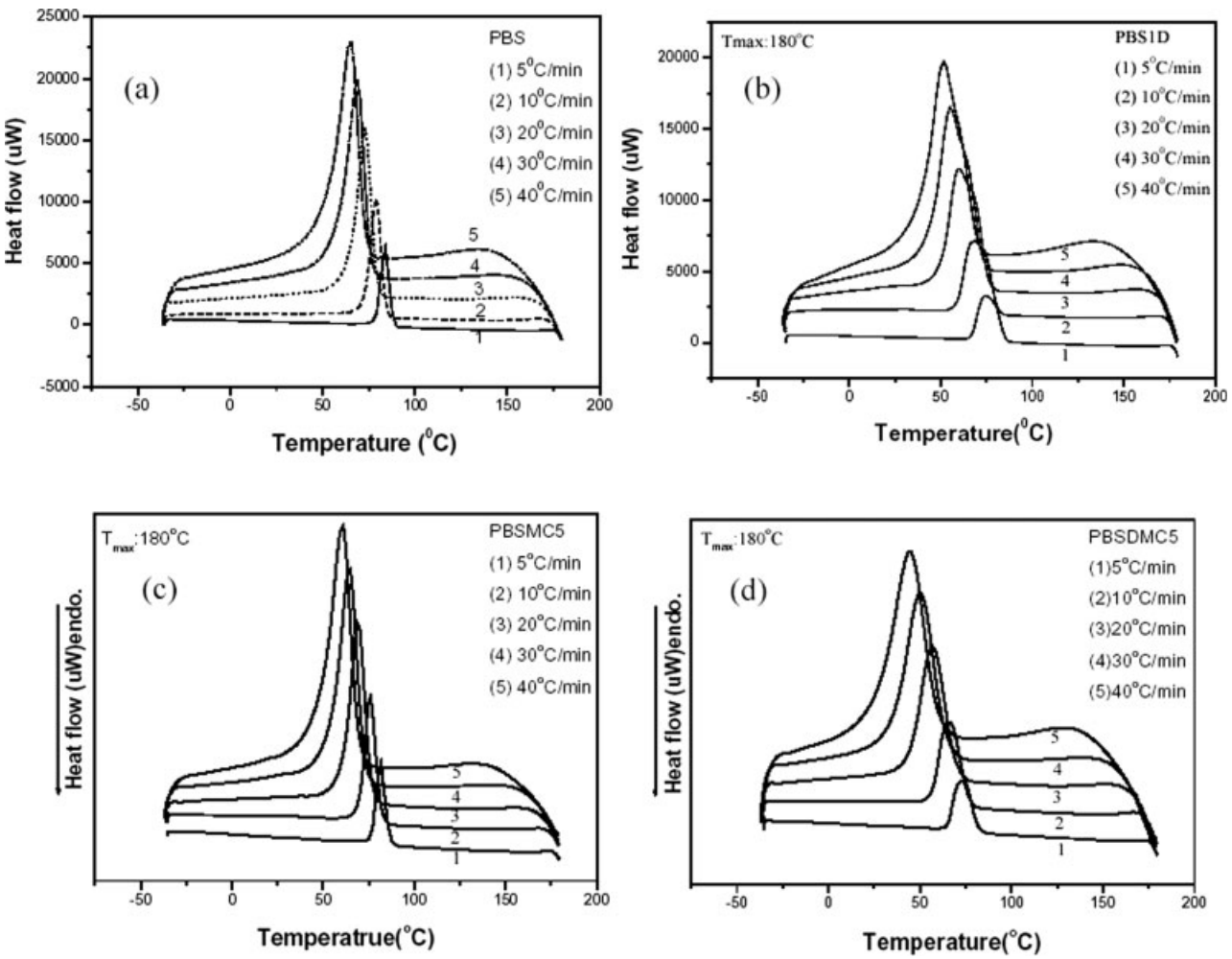

Figure 6 DSC thermograms of (a) PBS, (b) PBS1D, (c) PBSMC5, (d) PBSDMC5.

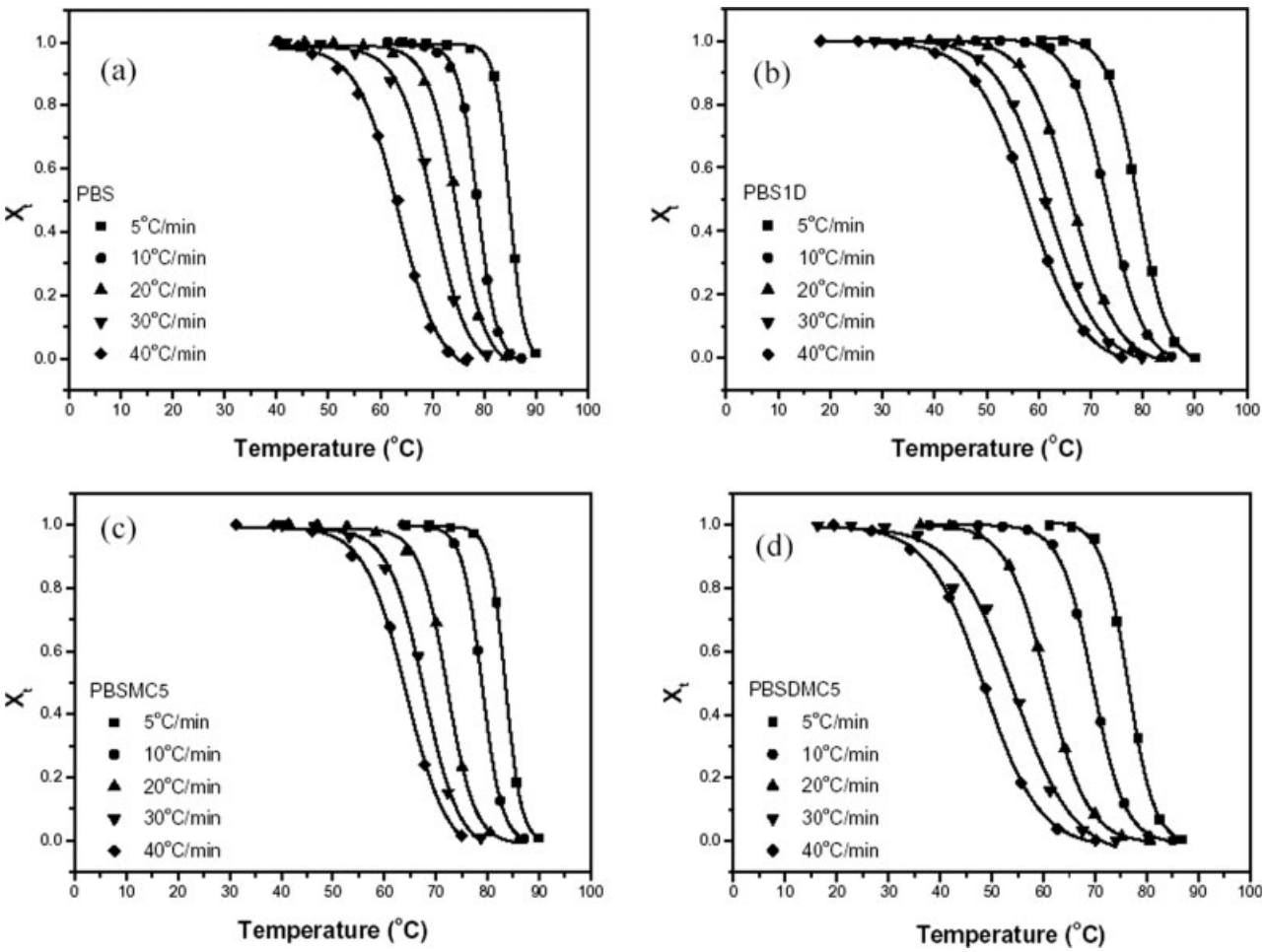

Figure 7 Plots of crystallinity (X_t) versus tempertaure (°C) for (a) PBS, (b) PBS1D, (c) PBSMC5, (d) PBSDMC5.

at the same cooling rate, correspondingly. This indicates that the crystallization rate was hindered by the cross-linking structure leading to the lower crystallization temperature and broader peak.

Figure 7(a–d) illustrates the relationship between the crystallinity and crystallization temperature, whereas Figure 8(a–d) shows the plots of $\ln(-\ln(1 - X_t))$ versus $\ln\varphi$ (Ozawa method) for the samples. Figures 8(a–d) would give a straight line if the Ozawa equation holds valid. $K(T)$ and m could be estimated from the intercept and the slope, respectively. However, some obvious zigzag lines were found, which is similar to those observed in literature.[20,31,34] This indicates that m and $K(T)$ are not constants with regard to temperature during the crystallization process. According to researches reported by Kong et al.,[34,35] the results showed why the Ozawa equation cannot describe well the nonisothermal crystallization behavior of polymers and composites. This is probably because of the improper assumption, such as the neglect of secondary crystallization in Ozawa's theory, and the quasi-isothermal nature of the treatment. Therefore, the Ozawa analysis could not adequately describe the nonisothermal crystallization kinetics of PBS and PBS/clay composites. The modified Avrami equation was subsequently adopted to analyze the nonisothermal crystallization behavior by Kong et al.[20,31,34] It was found that this method was indeed capable of describing the nonisothermal crystallization process.

While the cooling rate was constant, the horizontal temperature axis of Figure 7(a–d) could be transformed to time scale [Fig. 9(a–d)]. As indicated, the higher the cooling rate, the shorter the completed crystallization time. Moreover, as a result of the subsequent calculation by the modified Avrami equation, Figure 10(a–d) was obtained. The slopes (n) and intercepts (Z_t) of the lines at different cooling rates in the figure were also calculated (Table III). These kinetic parameters of crystallization at different cooling rates calculated by the DSC analysis and modified Avrami equation are shown in Table III. The results revealed that the crystallization temperature (T_c), the crystallization rate constants (Z_t and Z_c) and heat of crystallization (ΔH_c) were decreased with the addition of organoclay at the same cooling

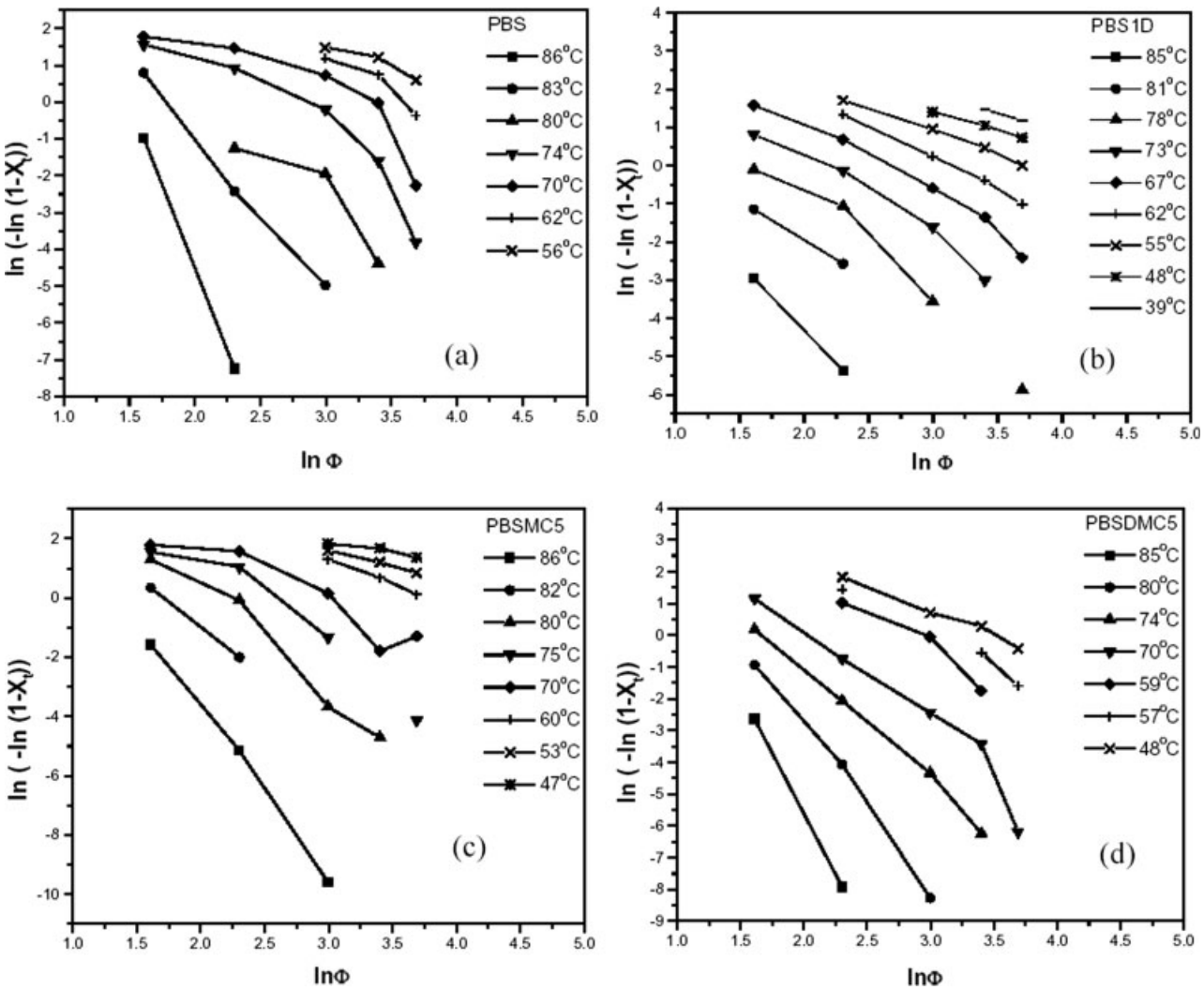

Figure 8 Plots of $\ln(-\ln(1 - X_t))$ versus $\ln\varphi$ (Ozawa method) for (a) PBS, (b) PBS1D, (c) PBSMC5, (d) PBSDMC5.

rate for uncross-linked samples (PBS, PBSMC5, and PBSMC10). On the other hand, the half-life of crystallization ($t_{1/2}$) was increased as a result of the addition. This is consistent with the results of other researches.[36,37] Via the addition of organoclay, Bionolle molecules were inserted into the layers of the organoclay, and subsequently the molecular motion of the polymer chain was possibly restrained by the clay with a high aspect ratio. The lower crystallinity seen in the nanocomposite is because of the inability of polymers chains to be fully incorporated into growing crystalline lamella. This leads to the smaller crystallization rate, lower T_c and crystallinity. Moreover, the crystallization temperature (T_c) and the crystallization rate constants (Z_t and Z_c) of cross-linked PBS1D were smaller than those of PBS. On the other hand, the half-life of crystallization ($t_{1/2}$) and heat of crystallization (ΔH_c) were larger than those of PBS. This indicates that the molecular motion of the polymer chain was possibly restrained by the network structure. The larger crystallinity seen in the PBS1D was possibly because of better alignment in the amorphous regions of PBS resulting from the cross-linking reaction.[38] According to the literatures,[38–43] it is suggested that the low dose irradiation results in intermolecular cross-linking and main-chain scission. The latter creates shorter polymer chain and reduces the number of entanglements per molecule which, in turn, increases molecular mobility. The increase in mobility permits the molecules to form crystallites in the amorphous regions. Short chains produced in the amorphous part can crystallize easier than the long ones; it is possible that they at least contribute partly to thickening of the already existing lamellae.

The results of cross-linked samples (PBSDMC5 and PBSDMC10) revealed that heat of crystallization (ΔH_c) was decreased with the addition of organoclay at the same cooling rate. Indeed, the lower crystallinity seen in the nanocomposite is because of the

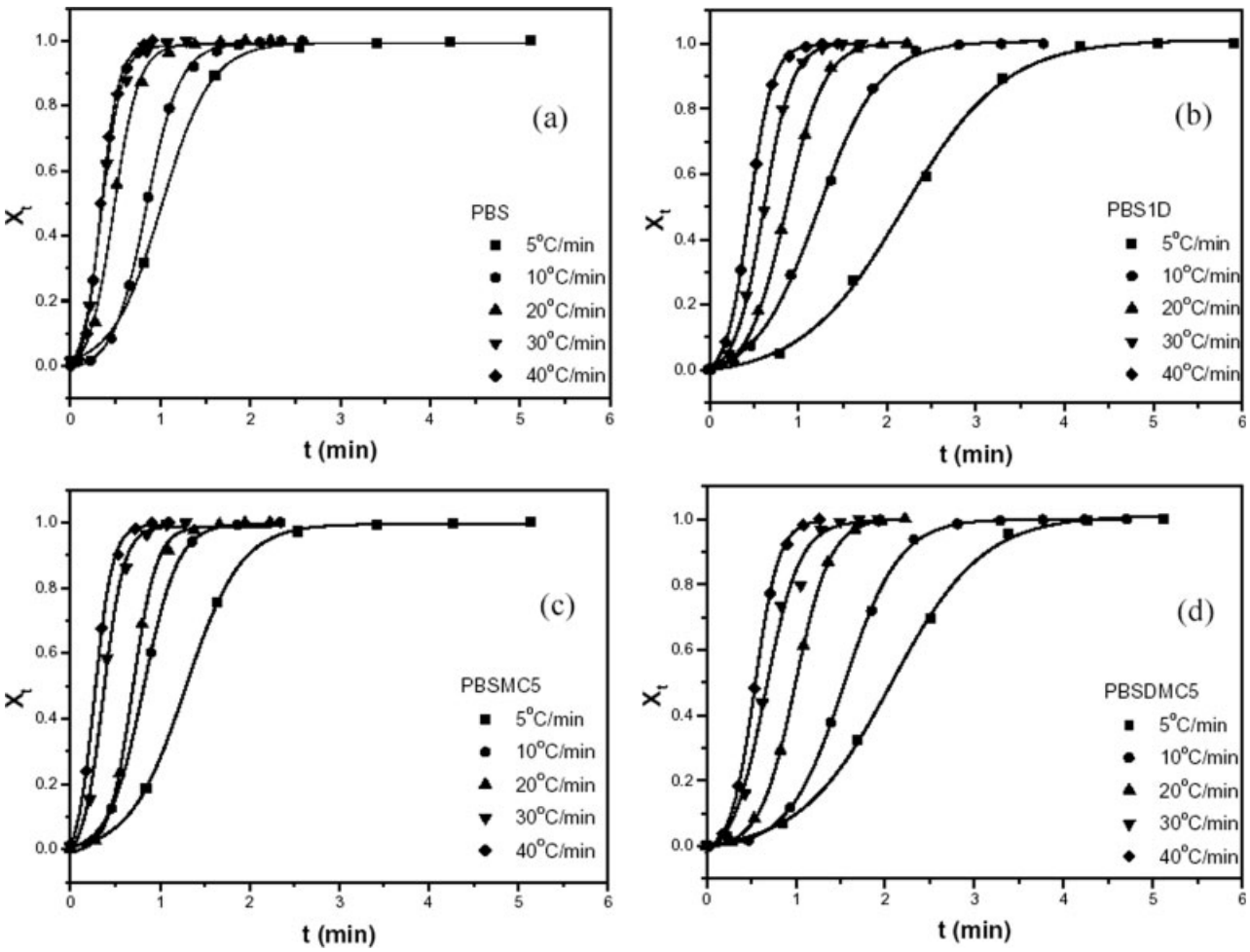

Figure 9 Plots of crystallinity (X_t) versus time (t) for (a) PBS, (b) PBS1D, (c) PBSMC5, (d) PBSDMC5.

inability of polymers chains to be fully incorporated into growing crystalline lamella. This is consistent with the phenomenon mentioned above. On the other hand, the crystallization temperatures (T_c), the crystallization rate constants (Z_t and Z_c), and the half-lives of crystallization ($t_{1/2}$) of PBS1D and PBSDMC5 were close to each other, but differed from those of PBSDMC10. This implies that the effect of cross-linking reaction influencing the crystallization rate is more pronounced than that of clay addition. Moreover, the addition of clay would hinder the cross-linking reaction.[44] Consequently, the crystallization rate of PBSDMC10 was slightly larger than those of PBS1D and PBSDMC5.

The values of n were between 2.44 and 2.64 for the pristine PBS sample, but those for PBSMC5 and PBSMC10 were between 1.86 and 3.08. This indicates that the crystal of Bionolle grew three dimensionally, resulting in the formation of spherulitic crystal.[45] On the other hand, the growth of crystallization was changed by the addition of organoclay. The crystallization behavior of PBSMC nanocomposites became a mixed type of two- and three-dimensional growth.[45] The heteronucleation phenomenon in the presence of organoclay would break the crystal structure of the polymer. This led to the formation of a mixture of circular and spherical crystals.[45] Similar phenomena were also found in the cross-linked samples. The values of n were between 2.24 and 2.68 for the nonclay-containing cross-linked PBS sample (PBS1D), but those for PBSDMC5 were between 2.59 and 3.19, and for PBSDMC10 between 1.81 and 2.62. This indicates that the crystallization behavior of PBSDMC nanocomposites also underwent the mixed type of two- and three-dimensional growth, resulting in the formation of a mixture of circular and spherical crystals.[45,46] A wider range of n was found for PBS1D than that of pristine PBS. This indicates that the different crystallization rates of cross-linked and uncross-linked molecules in the PBS1D sample would lead to the wider range of n and distorted crystal structure. Moreover, the values of n for PBSDMC10 and PBSMC10 were close to each other, but were smaller than that of PBSDMC5. This

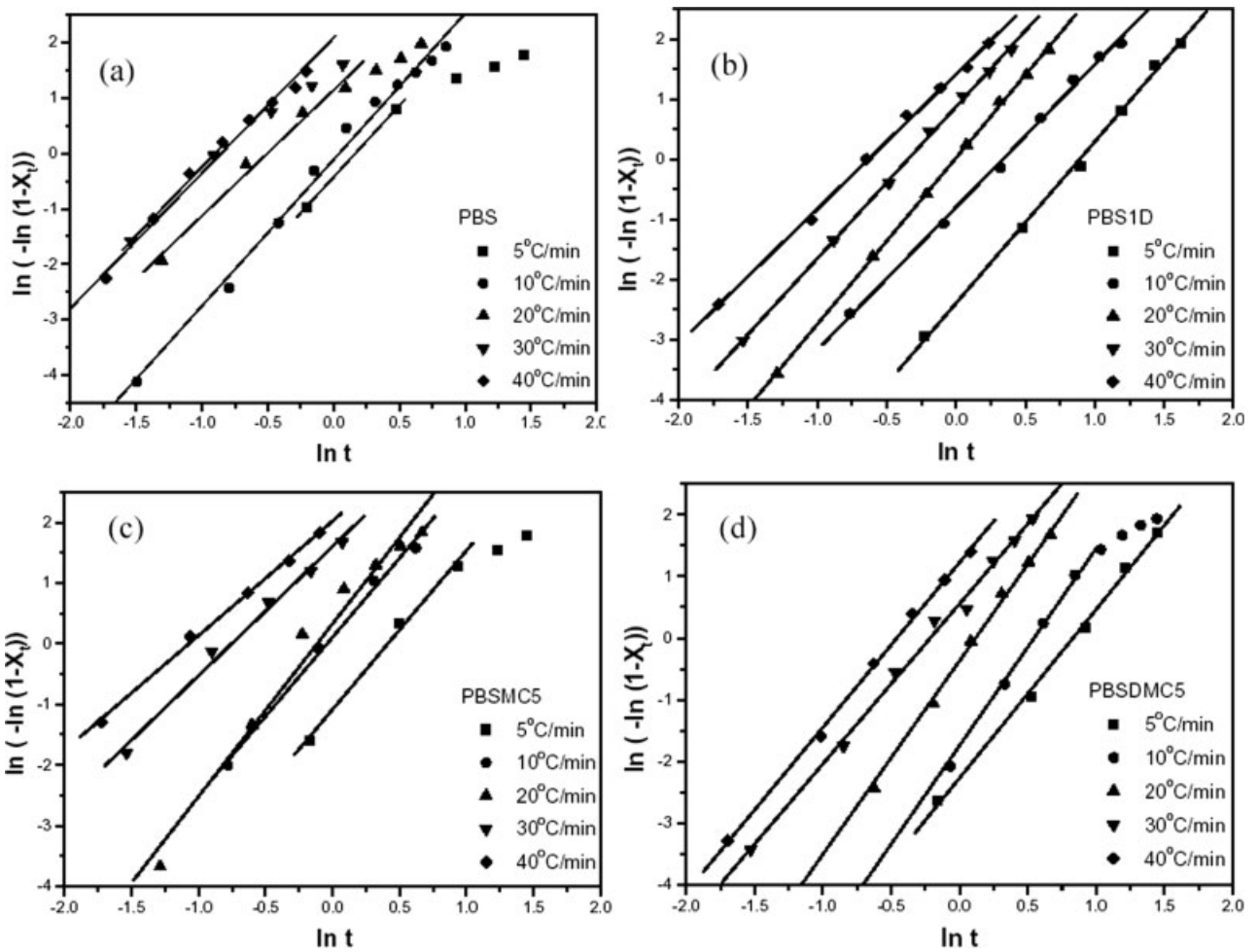

Figure 10 Plots of $\ln(-\ln(1 - X_t))$ versus lnt (modified Avrami method) for (a) PBS, (b) PBS1D, (c) PBSMC5, (d) PBSDMC5.

corroborated the results mentioned earlier, that the addition of clay would hinder the cross-linking reaction. Consequently, the crystal shape of PBSDMC10 was affected more extensively by the high-aspect-ratio-clay than by the cross-linking reaction, leading to a smaller value of n than those of PBS1D and PBSDMC5.

Polarizing optical micrographs

The optical micrographs of the crystalline growth at the crystallization temperature (T_c, 90°C) for the pristine Bionolle sample and uncross-linked nanocomposites are shown in Figure 11(a,b). The spherulites were found in the matrices of pristine Bionolle [Fig. 11(a)]. On the other hand, the smaller and less ordered crystals were found in the micrographs of the uncross-linked nanocomposites [Fig. 11(b)]. These results revealed that the dispersed clay particles acted as a nucleating agent to increase the number of the nuclei, causing the formation of smaller spherulites. The introduction of organoclay would influence the morphological structures of the Bionolle crystal such as spherulite size, shape, and nucleation density. This agrees with the DSC study. The addition of organoclay decreased the size of the spherulites, whereas the shape of the spherulites became irregular. Moreover, the optical micrographs of the cross-linked samples are shown in Figure 11(c,d). The distorted and compact spherulites were found in the matrices of cross-linked PBS1D sample [Fig. 11(c)]. This is consistent with the results of kinetic analysis of crystallization mentioned earlier. The compact alignment resulting from the cross-linking reaction led to larger crystallinity of PBS1D. However, the cross-linking reaction also brought about the distorted crystal structure. Smaller and less ordered crystals were also found in the micrographs of the cross-linked nanocomposites [Fig. 11(d)]. These phenomena were similar to those observed for the uncross-linked nanocomposites. The addition of organoclay decreased the size of the spherulites, whereas the shape of the spherulites would become irregular.

TABLE III
Kinetic Parameters of Crystallization for Samples at Different Cooling Rates

	Φ (°C min^{-1})	T_c (°C)	$t_{1/2}$ (min)	Z_t	Z_c	ΔH_c (J/g)	n
PBS	5	83.5	1.04	0.65	0.92	−79.1	2.58
	10	78.7	0.88	0.89	0.99	−78.1	2.64
	20	72.8	0.49	3.13	1.06	−76.9	2.27
	30	68.7	0.35	4.84	1.05	−76.3	2.48
	40	64.9	0.35	8.02	1.05	−75.9	2.44
PBSMC5	5	81.5	1.30	0.34	0.81	−75.7	2.62
	10	75.9	0.83	1.11	1.01	−74.0	2.6
	20	69.1	0.72	1.38	1.02	−73.4	2.84
	30	64.0	0.39	4.94	1.05	−71.5	2.12
	40	60.2	0.28	7.54	1.05	−69.3	1.89
PBSMC10	5	80.4	1.30	0.32	0.80	−67.4	2.81
	10	74.3	1.00	0.67	0.96	−66.5	3.08
	20	65.8	0.66	2.07	1.04	−64.9	2.7
	30	60.0	0.46	4.27	1.05	−63.9	2.36
	40	55.2	0.32	5.46	1.04	−62.4	1.86
PBS1D	5	74.3	2.20	0.09	0.62	−85.6	2.68
	10	68.5	1.27	0.45	0.92	−83.8	2.37
	20	61.1	0.87	1.03	1.00	−82.8	2.76
	30	55.2	0.61	2.40	1.03	−81.5	2.52
	40	51.5	0.47	3.15	1.03	−79.6	2.24
PBSDMC5	5	72.9	2.09	0.10	0.63	−74.8	2.73
	10	65.9	1.52	0.18	0.84	−72.9	3.19
	20	56.6	1.02	0.69	0.98	−72.1	3.13
	30	50.3	0.69	1.74	1.02	−71.7	2.59
	40	44.6	0.56	3.41	1.03	−71.4	2.67
PBSDMC10	5	78.8	1.39	0.30	0.79	−67.5	2.53
	10	73.1	1.05	0.60	0.95	−66.7	2.62
	20	65.1	0.63	1.85	1.03	−65.7	2.3
	30	59.1	0.39	4.28	1.05	−65.1	1.9
	40	53.8	0.34	5.13	1.04	−63.6	1.81

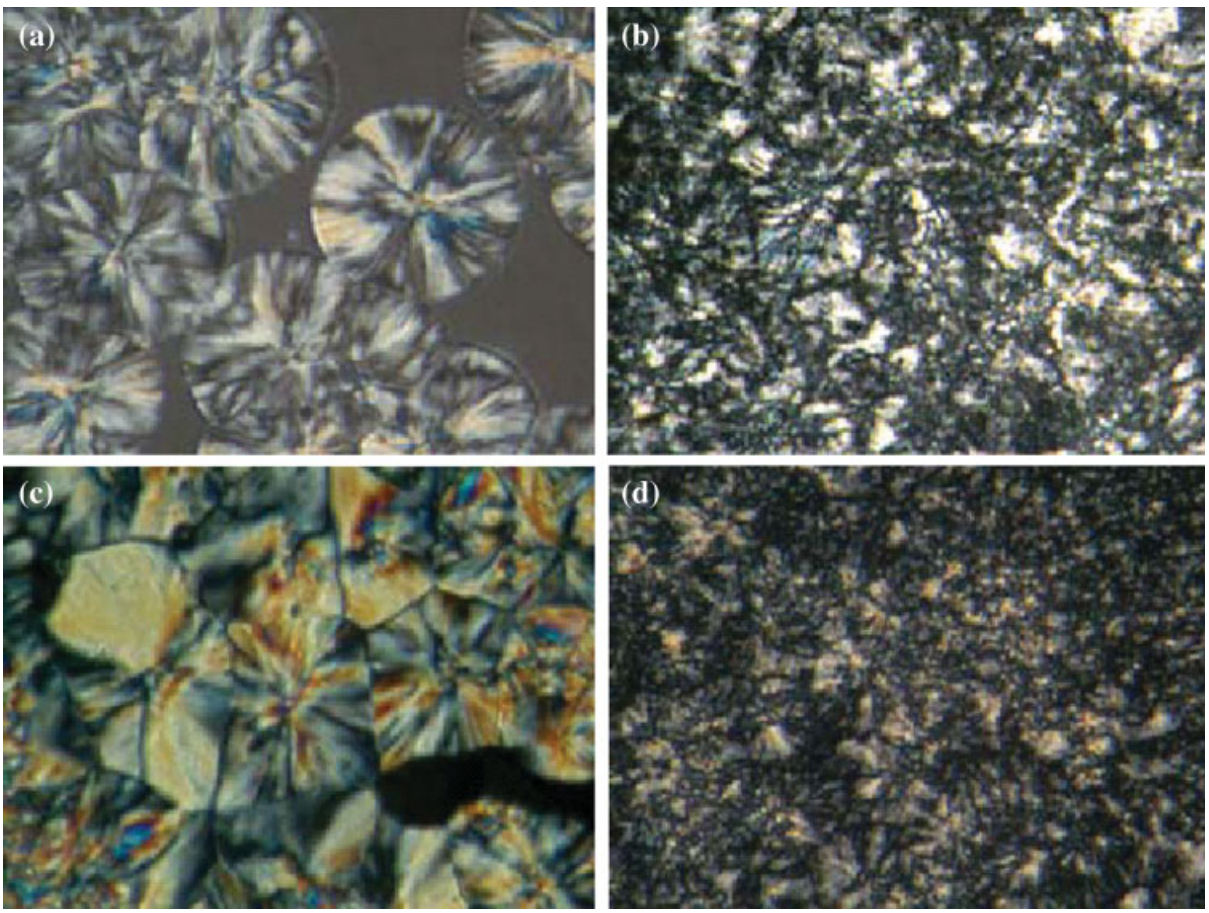

Figure 11 POM micrograph of (a) PBS, (b) PBS1D, (c) PBSMC5, (d) PBSDMC5. [Color figure can be viewed in the online issue, which is available at www.interscience.wiley.com.]

Gas permeability properties

Figure 12 and Table IV show the results of oxygen permeation test. Oxygen relative permeability (P_c/P_p) is obtained by dividing the oxygen permeability coefficient of samples with that of pristine PBS. The oxygen permeability coefficient was decreased with increases in the content of the organoclay, for both PBSMC and PBSDMC nanocomposites. When the content of organoclay reached 10% (PBSMC10 and PBSDMC10), the decrement of the oxygen permeability coefficient reached about 46.64% and 39.53%, respectively. It is important to note that the cross-linked network structure was not able to enhance the barrier property of PBS. The oxygen permeability coefficient of cross-linked PBS1D (0.252 Barrer) was larger than that of the pristine PBS sample (0.226 Barrer). Moreover, the decrements of oxygen permeability coefficient for the cross-linked PBSDMC nanocomposites (6.38 ~ 39.53%) also seemed smaller than those of uncross-linked PBSMC ones (23.87 ~ 46.64%). This may due to less homogeneity between the organoclay and cross-linked PBS, leading to a shorter path away from the cross-linked area. These results revealed that the gas permeability of PBS was effectively depressed by the addition of organoclay. In contrast, the cross-linked structure of polymer seemed not to be very effective in decreasing the gas permeability of PBS.

According to Ray and Okamoto's research,[47] the oxygen permeability coefficient of PLA could be decreased from 0.309 to about 0.264 ~ 0.273 Barrer (decrement: 14.56 ~ 11.65%) by the addition of 4 wt % different kinds of organoclay. In our study, the decrement of oxygen permeability coefficient can reach 32.49% by just adding of 3 wt % of organoclay (PBSMC3, Table IV). Moreover, the oxygen permeability coefficients of clear resins, such as poly(lactic acid) (PLA), high-performance polystyrene (HIPS), polyethylene terephthalate (PET), and polypropylene (PP) are 0.24, 1.80 ~ 2.40, 0.018 ~ 0.036, and 0.90 Barrer, respectively.[48] Table IV shows that the oxygen permeability coefficients of PBS and the composites are between 0.252 and 0.123, these values are competitive with those of PLA, HIPS, and PP, but still larger than that of PET.

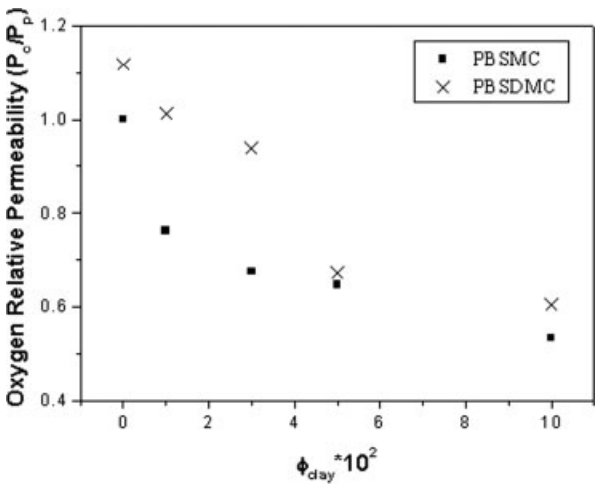

Figure 12 Oxygen permeation rates of the nanocomposites as a function of the organoclay contents.

TABLE IV
Oxygen Permeation Properties of Samples

	O_2 gas permeability coefficient (Barrer)	Decrement (%)
PBS	0.226	–
PBSMC1	0.172	23.87
PBSMC3	0.152	32.49
PBSMC5	0.146	35.17
PBSMC10	0.123	46.64
PBS1D	0.252	–
PBSDMC1	0.229	–
PBSDMC3	0.211	6.38
PBSDMC5	0.151	32.83
PBSDMC10	0.136	39.53

CONCLUSION

The results of XRD revealed that the organoclay (CPC/MMT) was further intercalated or exfoliated in the Bionolle matrices. The crystalline morphology of pristine Bionolle was found to be spherulite. On the other hand, the dispersed clay particles acted as a nucleating agent in the nanocomposites to increase the number of the nuclei, causing formation of smaller and irregular spherulites. Moreover, the cross-linking reaction is possibly capable of increasing the crystallinity through the compact alignment of the molecules. The results also revealed that both clay-addition and cross-linking effects retard the crystallization rate of the Bionolle molecules. It seems that the cross-linking feature is more effective than the clay-addition in the retardation. Moreover, better gas barrier properties of nanocomposites were achieved by the addition of organoclay, but not by the presence of cross-linked structure in polymers.

References

1. Ray, S. S.; Okamoto, K.; Okamoto, M. Macromolecules 2003, 36, 2355.
2. Fujimaki, T.; Harigaya, N. J. Jpn Soc Polym Process 1993, 5, 36.
3. Okamoto, K.; Ray, S. S.; Okamoto, O. J Polym Sci Part B: Polym Phys 2003, 41, 3160.
4. Chen, G. X.; Kim, E. S.; Yoon, J. S. J Appl Polym Sci 2005, 98, 1727.
5. Ray, S. S.; Okamoto, M. Prog Polym Sci 2003, 28, 1539.
6. Bharadwaj, R. K. Macromolecules 2001, 4, 9189.

7. Giannelis, E. P.; Krishnamoorti, R.; Manias, E. Adv Polym Sci 1999, 138, 107.
8. LeBaron, P. C.; Wang, Z.; Pinnavaia, T. J Appl Clay Sci 1999, 15, 11.
9. Yano, K.; Usuki, A.; Okada, A.; Kuruachi, T.; Kamigaito, O. J Polym Sci Part A: Polym Chem 1993, 31, 2493.
10. Yano, K.; Usuki, A.; Okada, A. J Polym Sci Part A: Polym Chem 1997, 35, 2289.
11. Giannellis, E. P. Adv Mater 1996, 8, 29.
12. Strawhecker, K. E.; Manias, E. Chem Mater 2000, 12, 2943.
13. Osman, M. A.; Mittal, V.; Morbidelli, M.; Suter, U. W. Macromolecules 2004, 37, 7250.
14. Ku, B. C.; Froio, D.; Steeves, D.; Kim, D. W.; Ahn, H.; Ratto, J. A.; Blumstein, A.; Kumar, J.; Samuelson, L. A. J Macromol Sci Pure Appl Chem 2004, 41, 1401.
15. Harris, J. J.; Derose, P. M.; Breuning, M. L. J Am Chem Soc 1999, 121, 1978.
16. Khonakdara, H. A.; Morshediana, J.; Wagenknechtb, U.; Jafarib, S. H. Polymer 2003, 44, 4301.
17. Martinez-Pardo, M. E.; Vera-Graziano, R. R. Phys Clrrm 1995, 45, 93.
18. Wang, T. Y.; Jeng, R. J.; Wu, J. Y.; Shih, Y. F.; Young, S. F.; Lai, Y. T.; Wang, L. L. In Proceedings of the 11th Annual APCChE, (paper I.D. 323), Kuala Lumpur, Malaysia, Aug 27–30, 2006.
19. Shih, Y. F.; Wang, T. Y.; Jeng, R. J.; Wu, J. Y. In Proceedings of the 30th Annual Conference on Polymer, Taipei, Taiwan, Jan 19–20, 2007.
20. Chen, G. X.; Yoon, J. S. J Polym Sci Part B: Polym Phys 2005, 43, 817.
21. Ohkita, T.; Lee, S. H. J Appl Polym Sci 2005, 97, 1107.
22. Ren, M.; Song, J.; Song, C.; Zhang, H.; Sun, X.; Chen, Q.; Zhang, H.; Mo, Z. J Polym Sci Part B: Polym Phys 2005, 43, 3231.
23. Ku, B. C.; Blumstein, A. L.; Samuelson, A.; Kumar, J.; Kim, D. W. In Encyclopedia of Nanoscience and Nanotechnology; Schwarz, J. A., Contescu, C., Putyera, K. Eds.; Marcel Dekker: New York, 2004, p 213.
24. Neto, C. G. T.; Dantas, T. N. C.; Fonseca, J. L. C.; Pereira, M. R. Carbohydr Res 2005, 340, 2630.
25. S.Pauly, In Polymer Handbook, 4th Ed.; Brandrup, J., Immergut, E. M., Grulke, E. A., Eds.; Wiley: New York, 1999, p 543.
26. Avrami, M. J. J Chem Phys 1939, 7, 1103.
27. Avrami, M. J. J Chem Phys 1940, 8, 212.
28. Avrami, M. J. J Chem Phys 1941, 9, 177.
29. Evans, U. R. Trans Faraday Soc 1945, 41 365.
30. Ozawa, T. Polymer 1971, 12, 150.
31. Liu, T.; Mo, Z.; Wang, S.; Zhang, H. Polym Eng Sci 1997, 37, 568.
32. Nakamura, K.; Katayama, K.; Amano, T. J Appl Polym Sci 1973, 17, 1031.
33. Jeziorny, A. Polymer 1978, 19, 1142.
34. Kong, X.; Yang, X.; Zhou, E. Polym Eng Sci 2001, 41, 786.
35. Eder, M.; Wlochowicz, A. Polymer 1983, 24, 1593.
36. Wu, D.; Zhou, C.; Fan, X.; Mao, D.; Bian, Z. J Appl Polym Sci 2006, 99, 3257.
37. Fornes, T. D.; Paul, D. R. Polymer 2003, 44, 3945.
38. Zhao, Z.; Yu, W.; Chen, X. Radiat Phys Chem 2002, 65, 173.
39. Lee, K. Y.; Lee, K. H. Wear 1999, 225–229, 728.
40. Pucic, I.; Jurkin, T. Radiat Phys Chem 2007, 76, 1318.
41. Stojanovic, Z.; Kacarevic-Popovic, Z.; Galovic, S.; Milicevic, D.; Suljovrujic, E. Polym Degrad Stab 2005, 87, 279.
42. Zainuddin, J.; Albinska, P.; Ulanski, J. M.; Rosiak, J. Radioanal Nucl Chem 2002, 253, 339.
43. Minkova, L.; Stamenova, R.; Tsvetanov, C.; Nedkov, E. Radiat Phys Chem 1989, 27, 621.
44. Sung, Y. T.; Kum, C. K.; Lee, H. S.; Kim, J. S.; Yoon, H. G.; Kim, W. N. Polymer 2005, 46, 11844.
45. Gedde, U. W. Polymer Physics, Chapter 8; Chapman & Hall: London, 1995.
46. Song, J.; Ren, M.; Song, C.; Wang, S.; Zhang, H.; Mo, Z. Polym Int 2004, 53, 1773.
47. Ray, S. S.; Okamoto, M. Macromol Rapid Commun 2003, 24, 815.
48. Leaversuch, R. http://www.ptonline.com/articles/200203fa2.html.